Stress Waves in a Damaged Rod Subjected to Longitudinal Impact

Hesham A. Elkaranshawy
Department of Engineering Mathematics and Physics, Alexandria University, Engineering Mechanics Division, Alexandria, Egypt
Email: hesham_elk@alexu.edu.eg

***Abstract*— In this paper simulated visualization of propagating waves in an elastic rod with damage is presented to enhance the understanding of the physical phenomenon and to identify damage location and severity. The rod has one end fixed and the other free end is subjected to impact of a rigid mass. Consequently, longitudinal impact wave is generated at the contact end and traveled through the rod. Rods with and without damage are examined. Finite element model is constructed and used to simulate the propagation of the waves. The mechanism of the generation and propagation of secondary waves due to the damage is revealed. Remarkably, it is observed that a standing stress wave is created and resides in at the damage location. The shape of the damage governs the shape of this standing wave. The influences of the width, the length, the depth, and the location of the damage on the created standing wave are examined. The effect of the arrival of the reflected waves to damage location on the peak of the standing wave is also investigated. The outcomes of this work give clarification to some practical observations and can be used for damage detection and assessment.**

***Index Terms*— damage detection; wave propagation; stress wave; longitudinal impact; finite element simulation**

I. Introduction

Damage detection becomes an important base for identifying the remaining life and integrity of a structure, a machine or a component. During the service life, damage detection is vital as it improves safety and maintains high performance and reliability for structures and machines. Significant efforts are made to obtain the size, shape and location of damage nondestructively. However, increasing needs for effective and economical detecting techniques are recognized.

Modal analysis based methods are widely used; examples include frequency shift, mode shape change, strain energy, and damage index [1-4]. Some of these methods can only predict the existence of the damage while others can predict the location of the damage also. The current system properties are compared to the properties of the undamaged system and link the changes to damage. For slight damage, the changes in properties of the damaged system could be insignificant and even fall within measurement error, which reduces the effectiveness of the prediction. Typically, precise measurements are necessary and high computational efforts are required.

Wavelet analysis is successfully used in damage detection (for example see [5-7]). Wavelet analysis is capable of revealing some hidden aspects of the data that other analysis techniques fail to detect; therefore, small damages can be detected clearly. However, it is not easy to choose the wavelet that can detect the damage suitably. Never less, the wavelet transform produces quite poor frequency resolution in high frequency regions.

Detection methods based on propagation of elastic waves capture great interest and are observed as encouraging solutions to damage diagnosis [8-13]. Once a diagnosis wave propagates in the component, parameters that characterize the wave travel are interpreted. The analysis of the response can determine the existence of damage, the location of it, and its severity. The choice of the excitation wave is critical. For instant, small wavelength is required to capture small damage. Effect of the analysis of higher harmonics on the detection is discussed in [12]. Ultrasonic waves were used in [9,13] and a good review can be checked in [10].

Palacz and Krawczuk [14] constructed signals by multiplication of different sinusoidal functions by a triangle to provide the effect of a pulse. A harmonic motion was used to modulate a transverse triangular force impulse by Akbas [15]. A pulse can excite a wide range of frequencies; hence, it can detect damage even if it is very small. A pulse can be created using an impact hammer. Although an impact hammer is simple and inexpensive, it is impractical to control the created pulse or to replicate it. A controllable and replicable pulse can be created for a rod through the struck of a rigid mass with the rod [16]. Bajabaa and Elkaranshawy [17] proposed the use of this pulse for damage detection in rods. Time variation of contact force, velocity, and stress at the contact end are monitored.

Though wave propagation methods for damage detection are the focus of a significant amount of research work, the characteristics of the propagating wave itself did not receive the same attention. In this paper the mechanism of generation of secondary waves due to the damage in rods is investigated. Finite element model is constructed and a simulated visualization of the propagation of the impact wave through the bar is

Manuscript received March 4, 2018; revised March 15, 2019.

doi: 10.18178/ijmerr.8.3.488-493

monitored. The observed standing stress wave at the damage location is checked and examined. The relation between the shape of the standing wave and the shape of the damage is considered. The effect of the arrival of reflected waves to damage location on the peak of the standing wave is also investigated. The outcomes of this work enhance the understanding of the complicated physical phenomenon, explain some practical observations, and can be used for damage detection and assessment.

II. Wave Propagation

It is assumed that the rod has mass m, Young's modulus E, density ρ, cross- sectional area A and length *l*. The rod is initially at rest and is struck on the right end $x = l$ at the initial time $t = o$ by a moving rigid mass m_0 with initial velocity υ_0. The damage is located at distance *e* from the fixed end. The displacement of the rigid mass at time t is donated by $q(t)$ and the displacement on the rod at position x and time t is given by $u(x,t)$, as in Fig. 1.

The governing equation for the longitudinal wave in the rod is

$$\frac{\partial^2 u(x,t)}{\partial t^2} = c^2 \frac{\partial^2 u(x,t)}{\partial x^2} \tag{1}$$

where c is the wave propagation velocity

$$c = \sqrt{\frac{E}{\rho}} \tag{2}$$

According to St. Venant's principle, as contact established between the mass and the rod, both the mass and the contact end of the rod ($x = l$) are assumed to have the same velocity υ_0. Therefore, a compression wave is created in the rod. The wave travels along the rod and reflected at the other end ($x = 0$). During contact period, displacement $q(t)$ and velocity $\dot{q}(t)$ of the mass are the same as those of the contact end of the rod ($x = l$). The contact persists as long as the contact force *F(t)* between the mass and contact end of the rod does not vanish. The contact force equals the stress at the contact end times the rod's cross-sectional area i.e.

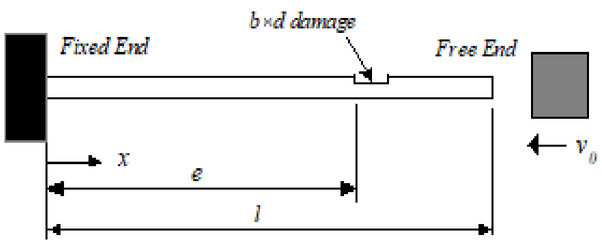

Figure 1 Longitudinal impact of a mass on a rod with damage

$$F(t) = EA \frac{\partial u(l,t)}{\partial x} \tag{3}$$

The motion of the rigid mass is governed by

$$m \frac{d\dot{q}}{dt} = F(t) \tag{4}$$

Equations (1), (3), and (4) are the equations of motion of the rod and the rigid mass during the impact period. After the cease of impact, the motion of the rod is controlled by equation (1), in the same time, since *F(t)* vanishes, equation (4) declares that the rigid mass moves with a constant velocity.

The pre-mentioned differential formulation of the equations of motion is equivalent to integral formulation, which requires the application of Lagrange's equation of motion. The finite element shape functions $[N(x)]$ link the displacement u to nodal displacement vector $\{U\}$ through

$$u(x,t) = [N]\{U\} \tag{5}$$

Consequently, the Lagrange's equation of motion leads to

$$[M]\{\ddot{U}\} + [K]\{U\} = \{f(t)\} \tag{6}$$

$[M]$ and $[K]$ are the global mass and stiffness matrices and $\{f(t)\}$ is the global force vector. $\{f(t)\}$ contains only the nodal forces due to the contact force, *F(t),* at the contact end and the rest of the vector is full of zeros. Equations (3) and (5) give

$$F(t) = EA\left[\frac{\partial N}{\partial x}(x = l)\right]\{U\}_{el} \tag{7}$$

where $\{U\}_{el}$ is the nodal displacement vector for the last element, which is the element in contact with the rigid mass. Equations (6) and (7) are the finite element equations of motion during impact for the rigid mass and the rod. The rod could be with or without damage, given that proper area for each element in the mesh is used. Due to the motion of the rigid mass, rigid body modes exist, therefore, through [*M*] is positive definite matrix, [*K*] is positive semi-definite matrix.

Newmark implicit time stepping method (Bathe [18]) is used to express the current velocity $\{\dot{U}\}_{N+1}$ and acceleration $\{\ddot{U}\}_{N+1}$ in terms of the current displacement $\{U\}_{N+1}$ and previously determined values of displacement $\{U\}_N$, velocity $\{\dot{U}\}_N$, and acceleration $\{\ddot{U}\}_N$. Combining these equations with the equations of motion (6) and (7) yields a system of algebraic equations in terms of $\{U\}_{N+1}$ and $F(t)_{N+1}$. Newton–Raphson iterative method (Bathe [1]) is used to solve the resulting equations to find the current displacement and contact force. The displacement and other variables' distributions in the rod at the end of impact serve as the initial conditions for the subsequent free vibrations of the rod, which are governed by the solution of equation (6) while equation (7) is no longer relevant.

III. Numerical Simulation

Numerical simulations for a rigid mass collides with a free-fixed elastic rod without and with damage are presented in this section, see Figure 1. The rod is an aluminum rod with a depth $D = 3$ *mm*, a width $w = 25$ *mm*, a length $l = 200$ *mm*, Young's modulus $E = 70$ *GN/m*^{2}, and mass density $\rho = 2710$ *kg/m*^{3}. For the rod with damage, the damage is located at distance $e = 20$ *mm* or *100 mm.* A third location is also considered where the damage is *20 mm* from the contact end. The depth of the damage 'd' is *10%, 20%, 30%, 40%,* or *50%* of the total depth of the rod *D*. The damage covers the width of the rod and its length 'b' is 4 mm or 8 mm. Thus, thirty different cases are considered for the rod with damage.

The rigid mass has the same mass as the rod. The mass moves towards the rod with initial velocity of $v_0 = 1$ *m/s*. Fifty elements are used to model the rod in the finite element model. The elements are two-nodes and one-dimensional linear elastic elements. A slight numerical damping is introduces through Newmark parameters ($\alpha = 0.52$, $\beta=0.2605$). The axial rigidity '*EA*' for elements used to model the damage is less than the axial rigidity of other elements used to model other parts of the rod to reflect the decrease in area for the damage region.

IV. Results and Discussions

The strength of the impact pulse depends on the mass ratio between the rod and the rigid mass, the impacting velocity of the mass, and material properties of the rod *A*, *E*, and ρ. Therefore, this impact pulse can be standardized, which is critical for comparing results and extracting practical information from them.

Employing St. Venant's principle, as contact starts the velocity of the contact end becomes immediately equals to the rigid mass velocity and right away a compression wave is created at the contact end and travels across the rod with velocity '$c = 5082.35$ *m/s*'. The time for the wave to travel across the rod from one end to the other end is $\tau = l/c = 3.935\times10^{-5}\,s$. The initial compression stress at the contact end is $\sigma_0 = -v_0\sqrt{E\rho}$ or *-13.77* MPa.

Using the present finite element simulation, visualization for the stress wave propagation in the rod is presented in Figs. 2 and 3 for a rod without damage and a rod with damage, respectively. The damage is located at *20 mm* from the contact end with a dimensionless depth of 0.4 and a length of 4mm. The two figures present the distribution of the dimensionless stress $c\sigma/E\,v_0$ over the rod length, with respect to the dimensionless time ct/l every time step of *0.0938*. Since the contact is not terminated yet, the contact end operates as a fixed end and the compression wave is reflected from that end as a compression wave again, as can be seen Figs. 2 1nd 3. For the rod with damage a mechanism for creation and propagation of secondary stress waves is initiated. Though the previously mentioned mechanism can be seen in Figure 3, an obvious outcome is obtained by comparing the stresses in rods with and without damage.

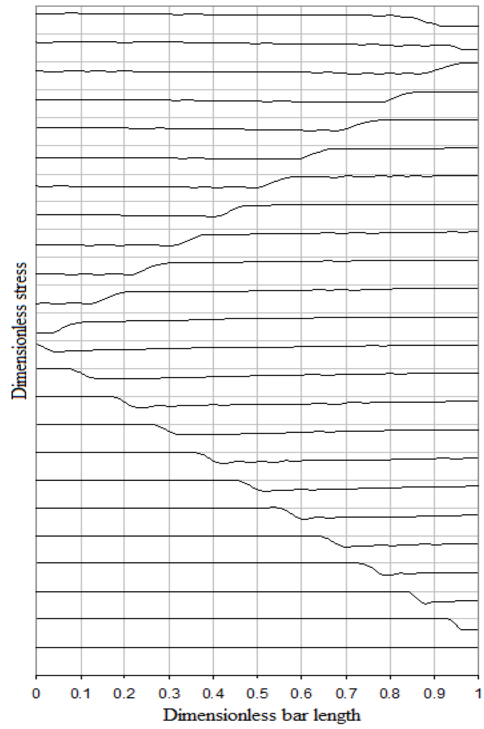

Figure 2 Propagation of stress wave along a rod without damage. Stress distributions are shown every 0.0938 dimensionless time

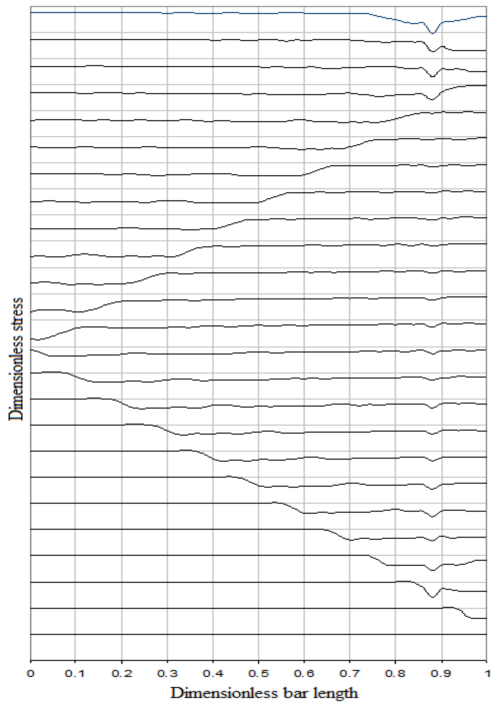

Figure 3 Propagation of stress wave along a rod with damage. Stress distributions are shown every 0.0938 dimensionless time

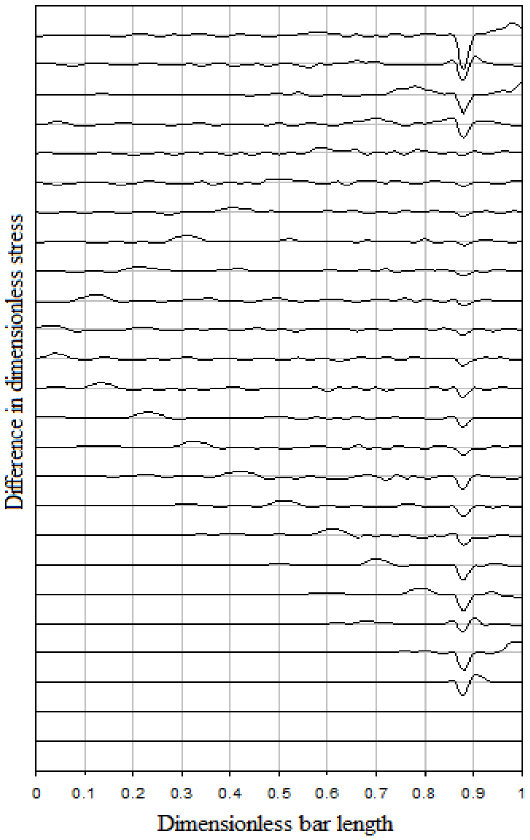

Figure 4 Propagation of difference between dimensionless stress in a rod with damage and a rod without damage. Stress differences are shown every 0.0938 dimensionless time

Table I shows the stress at the damage location for the rod without damage and with damage. Figure 4 shows the distribution of the difference between the signals in Figs. 2 and 3. In practical conditions some misleading circumstances are found when the stress measured at a specific point in a damaged rod is above the corresponding stress in undamaged rod. Mistakenly, it could be interpreted as a location of damage, but actually it is far from damage location and it is due to the propagation of secondary stress waves; for example, see Hu et al. [4].

TABLE I STRESS AT THE LOCATION OF THE DAMAGE

Dimensionless time	dimensionless stress		Dimensionless time	dimensionless stress	
	With damage	Without damage		With damage	Without damage
0.0938	0	0	1.3132	-0.34052	-0.24649
0.1876	0	0	1.407	-0.34052	-0.18957
0.2814	-1.07898	-0.45436	1.5008	-0.2836	-0.17077
0.3752	-0.87061	-0.58701	1.5946	-0.2836	-0.15196
0.469	-0.79488	-0.30291	1.6884	-0.26479	-0.15145
0.5628	-0.71915	-0.56821	1.7822	-0.24599	-0.15145
0.6566	-0.68154	-0.51128	1.876	-0.17026	-0.11334
0.7504	-0.64343	-0.34103	1.9698	-0.13214	-0.13265
0.8442	-0.54889	-0.37864	2.0636	-1.04137	-0.45436
0.938	-0.51128	-0.41624	2.1574	-1.06018	-0.71915
1.0318	-0.47317	-0.30291	2.2512	-1.38189	-0.51128
1.1256	-0.39744	-0.30291	2.345	-1.53334	-1.17402
1.2194	-0.37864	-0.32171			

A unique phenomenon takes place in stress wave in a rod with damage. As can be seen in Figs. 3 and 4, at the instant the front of the stress wave crosses the location of damage, a standing wave is created exactly at that location. It stayed there all the time, but its peak value decreases with time until the front of the original stress wave reaches the location of damage after reflection at the fixed end. At that instant its peak value immediately increases. The first reflected wave from the damage could be seen, moving first to the right and then to the left after reflected from the contact end. Many secondary waves are created and travel in the rod in the same way, as can be seen in Figure 4. Tough the peak of the standing wave at the location of the damage is tends to decrease with time, limited increase of its value occurs whenever a secondary wave across the damage. A major increase takes place when the reflected main wave and the first secondary wave returned back to the damage location.

A finite element simulation is performed to investigate the effect of damage depth, length and location in the outcome stress waves. In this simulation, three locations for damage are considered: e_1 *= 20 mm*, e_2 *= 100 mm*, and e_3 *= 176 mm i.e. 20 mm* from the contact end. For each case the length of the damage could be *4 mm* or *8 mm*. For each damage length, the dimensionless depth of the damage (d/D) could be 0.1, 0.2, 0.3, 0.4 and 0.5. The effects of damage depth and length are shown in Fig. 5. The damage located at e_1 *= 20 mm* and the simulation is performed for the two damage lengths and for each length the five damage depths. The peak stress of the standing wave increases with the increase of damage depth and the decrease of damage length. The effect of the damage location is shown in Fig. 6. The damage length is *4 mm* and the simulation is performed for the three damage locations and for each location the five damage depths. As expected, the peak stress of the standing wave increases with the increase of damage depth. However, the peak stress of the standing wave is higher at the two locations closed to the two ends of the rod than at the location closed to the midpoint of the rod.

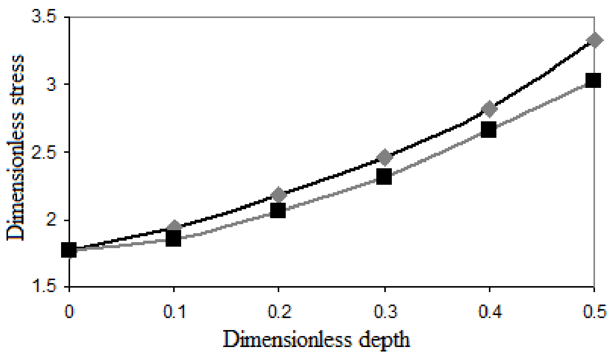

Figure 5 Relation between depth of damage and peak stress of the standing wave. Damage at e_1 *= 20 mm*: ♦ damage length *4 mm* and ■ damage length *8 mm*

These results and observations can be used to detect the damage, to locate its position, and to measure its severity. Once the measured stresses are higher than the corresponding stresses in an undamaged rod, damage is

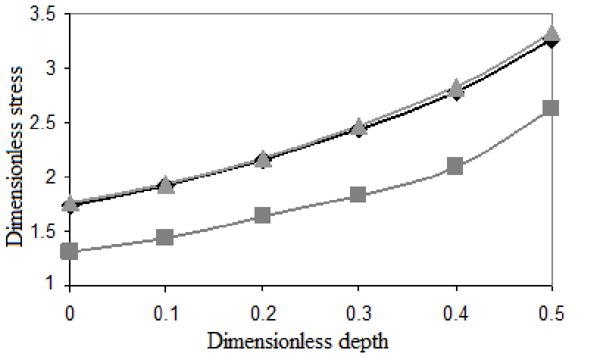

Figure 6 Relation between depth of damage and peak stress of the standing wave. Damage length is *4 mm*: ♦ $e_1 = 20$ *mm*, ■ $e_2 = 100$ *mm*, and ▲ $e_3 = 176$ *mm*

detected in the rod. The location where the stress is always higher than the corresponding stress in an undamaged rod and its peak value is significantly high is the location of damage. The width of the damage is exactly the width of the standing stress wave where the stresses are clearly higher than the corresponding stresses in an undamaged rod. A finite element simulation can be used to get the depth of the damage.

V. Conclusions

In this research work, wave propagation in a rod with damage has been considered. An impact pulse has been created at the free end of the rod by a projectile mass while the other end is fixed. The analytical equations of motion are presented utilizing St. Venant classical impact model. The corresponding finite element equations are derived, numerical scheme is constructed, and simulated visualization of the propagating waves through the rod has been developed. The visualization shows that a part of the wave created at the contact end is reflected from the damage. That reflected wave is reflected again from the contact end and travels in the rod in the same way as the original wave. Again a part of it is reflected from the damage. Many secondary waves are created and travel in the rod through this mechanism. Hence, the reasons behind the misleading situation when stress measured at a specific point far from damage location is above the corresponding stress in undamaged rod have been identified.

It has been realized that once the stress wave crosses the damage location a standing wave is created and exists in there all the time. The peak of this standing wave decreases with time but limited increase happens whenever a secondary wave across the damage and a major increase takes place when the reflected main wave and the first secondary wave across the damage location. It has been observed that the shape of the standing wave depends on the shape of the damage. The width of this wave is exactly the width of the damage. The increase of damage length decreases the maximum peak of the standing wave, while the increase of the damage depth increases the maximum peak of the standing wave. The maximum peak for damage closed to rod ends is higher than that for damage at mid of the rod.

As a direct conclusion of this analysis, the stress waves are superior to other waves in detecting damages. The outcomes can be used to detect the damage, to locate its position, and to measure its severity. This analysis contributes to the understanding of the propagation and reflection mechanism of waves due to damages.

References

[1] A. Messina, I.A. Jones, E.J. Wiliams, “Damage detection and localization using natural frequency changes,” *Proceedings of the First Conference on Structural Identification*, Cambridge, 1992, pp. 67–76.

[2] G. W. Housner, L. A. Bergman, T. K. Caughey, A. G. Chassiakos, R. O. Claus, S. F. Masri, R. E. Skelton, T. T. Soong, B. F. Spencer, and J. T. P. Yao, “Structural Control, Past Present and Future,” *Journal of Engineering Mechanics*, ASCE, vol. 123, no. 9, pp. 897-971, 1997.

[3] P. Cornwell, S. W. Doebling, and C. R. Farrar, “Application of the strain energy damage detection method to plate-like structures,” *Journal of Sound and Vibration*, vol. 223, no. 2, pp. 359-374, 1999

[4] H. Hu, B. Wang, C. Lee, and J. Su, “Damage detection of surface cracks in composite laminates using modal analysis and strain energy method,” *Composite Structures*, vol. 74, pp. 399-405, 2006.

[5] N. S. Bajabaa, "Multiple damage detection in structures using a coupled modal analysis and wavelet transform technique," Ph.D dissertation, University of central Florida, 2003.

[6] S. S. Law, X. Y. Li, X. Q. Zhu, and S. L. Chan, “Structural damage detection from wavelet packet sensitivity,” *Engineering Structures*, vol. 27, pp. 1339-1348, 2005.

[7] D.M. Joglekar, M. Mitra, "Analysis of flexural wave propagation through beams with a breathing crack using wavelet spectral finite element method," *Mechanical Systems and Signal Processing*, vol. 76-77, pp. 576-591, 2016.

[8] K.A. Lakshmanan, D.J. Pines, “Modelling damage in composite rotorcraft flex beams using wave mechanics,” *Smart Materials and Structures*, vol. 6, pp. 383–392, 1997.

[9] Z. Li and Y. H. Berthelot, “Propagation of transient ultrasound in thick annular waveguides: modeling, experiments, and application to crack detection,” *NDT&E International*, vol. 33, pp. 225-232, 2000.

[10] D. Broda, W.J. Staszewski, A. Martowicz, T. Uhl, and V.V. Silberschmidt, "Modelling of nonlinear crack–wave interactions for damage detection based on ultrasound—A review," *Journal of Sound and Vibration*, vol. 333, pp. 1097–1118, 2014.

[11] P. Kudelaa, M. Krawczuk, W. Ostachowicza, “Wave propagation modelling in 1D structures using spectral finite elements,” *Journal of Sound and Vibration*, vol. 300, pp. 88–100, 2007.

[12] D. Broda, L. Pieczonka, V. Hiwarkar, W.J. Staszewski, V.V. Silberschmidt, "Generation of higher harmonics in longitudinal vibration of beams with breathing cracks," *Journal of Sound and Vibration*, vol. 381, pp. 206-219, 2016.

[13] A.K. Singh, B. Chen, V. B.C. Tan, T. Tay, H. Lee, " Finite element modeling of nonlinear acoustics/ultrasonics for the detection of closed delaminations in composites," *Ultrasonics*, vol. 74, pp. 89-98, 2017.

[14] M. Palacz, M. Krawczuk, “Analysis of longitudinal wave propagation in a cracked rod by the spectral element method,” *Computers and Structures*, vol. 80, pp. 1809–1816, 2002.

[15] S.D. Akbas, "Wave propagation in edge cracked functionally graded beams under impact force, Journal of Vibration and Control, vol. 22, no. 10, pp. 2443–2457, 2016.

[16] H. A. Elkaranshawy and N. S. Bajaba, “A Finite element simulation to longitudinal impact waves in elastic rods,” *International Journal of Applied Engineering Research*, vol. 3, no. 6, pp 847-860, 2008.

[17] N. Bajaba and H. A. Elkaranshawy, “Damage detection in an elastic rod using finite element simulation to longitudinal impact waves,” *15th International Congress on Sound and Vibration*, Daejeon, Korea, 6-10 July 2008, pp. 1506-1513.

[18] K-J Bathe, *Finite Element Procedures*, Prentice Hall, Upper Saddle River, 1996.

Hesham A. Elkaranshawy was born in Alexandria, Egypt in 1961. He received his BSc degree (distinction with degree of honor) in mechanical power engineering and MSc degree in Engineering Mathematics from Alexandria University, Alexandria, Egypt, in 1983 and 1988 respectively. He received his PhD degree in Mechanical Engineering from McMaster University, Hamilton, Ontario, Canada, in 1995. During 1995-1996 he joined CAE Electronics, Montreal, Canada, as a Finite Element Specialist where he involved in design of the company's flight simulators and in its role in the world space station project. He became an ASSISTANT PROFESSOR at Department of Engineering Mathematics and Physics, Engineering Mechanics division, Alexandria University in 1996. In 1998 he established Dynamica Engineering Consultants, Giza, Egypt. In 2001, He became an ASSISTANT PROFESSOR at Department of Mechanical Engineering, Yanbu Industrial College, Royal Commission for Jubail and Yanbu, Saudi Arabia. Since 2010 he went back to Alexandria university and he is now a candidate for the position of PROFESSOR of Engineering Mechanics at Department of Engineering Mathematics and Physics.

Prof. Elkaranshawy was a board member of the Egyptian Syndicate for Engineers in Behera province. Many of his scientific papers are published in international journals. His research interests include multibody dynamics, robot dynamics, contact-impact dynamics, finite element modeling, mechanical vibrations, wave propagation, fault detection, ordinary differential equations and nonlinear systems.